Microchimica Acta (2021) 188: 364
https://doi.org/10.1007/s00604-021-05026-2

ORIGINAL PAPER

A simple strategy for signal enhancement in lateral flow assays using superabsorbent polymers

Taeyeong You[1,2] · Woojin Jeong[1,2] · Hwankyu Lee[3] · Yun Suk Huh[1,2,4] · Sun Min Kim[1,2,5] · Tae-Joon Jeon[1,2,4]

Received: 6 July 2021 / Accepted: 11 September 2021 / Published online: 6 October 2021

Abstract

To enhance the sensitivity of lateral flow assays (LFAs), a simple strategy is proposed using a nitrocellulose membrane modified with a superabsorbent polymer (SAP). SAP was incorporated into a nitrocellulose membrane for the flow control of detection probes. When absorbing aqueous solutions, SAP promoted the formation of biomolecule complexes to achieve up to a tenfold sensitivity improvement for the detection of human IgG. The assay time was optimized experimentally and numerically to within 20 min using this strategy. Moreover, fluid saturation in LFAs modified with SAP was mathematically simulated to better understand the underlying process, and molecular dynamics simulations were carried out to determine the effect of SAP. The proposed design was also applied to samples spiked with human immunoglobulin-depleted serum to test its applicability. The strategy presented is unique in that it preserves the characteristics of conventional LFAs, as it minimizes user intervention and is simple to manufacture at scale.

Keywords Lateral flow assay · Superabsorbent polymer · Sensitivity enhancement · Flow control · Colorimetric detection · Paper-based biosensor

Introduction

Paper-based in vitro diagnostics (lateral flow assays, dipsticks, microfluidic paper-based analytical devices; μPAD, etc.) are well suited to the WHO standard criteria for point-of-care testing (POCT) [1–3] and have made significant advances to date [4–8]. One of the most frequently used paper-based in vitro diagnostic methods is the lateral flow assay (LFA). LFAs have been widely used in quantitative and qualitative analysis in hospitals, physician offices, and clinical laboratories, as well as for personal uses due to their simplicity of operation and cost effectiveness [9]. Basic LFA techniques observe the signals of samples by using capillary movement. Analytes are dropped into a sample pad, and then moved to a conjugation pad smeared with detection antibodies have for analytes. The sample solution passes all the way along the membrane, and signals appear in the control line and test line with the immobilized receptors, i.e., antibodies [10].

Despite the advantages of the LFA, several studies to enhance its sensitivity and signal have been performed due to its relatively low accuracy (cross-reactivity, a high limit of detection, etc.). Therefore, a number of studies have been performed to increase the binding force of receptor molecules to slow the reaction time, which increases the signal readout. First, "wax patterning (printing)" methods are described in many studies. Carrilho et al., Renault et al., and Sena-Torralba et al. demonstrated that a hydrophobic barrier formed by the wax patterning method can control fluid flow [11–13]. Similarly, Preechakasedkit et al. developed a "wax-delayed channel" to delay the flow of the existing

✉ Yun Suk Huh
yunsuk.huh@inha.ac.kr

✉ Sun Min Kim
sunmk@inha.ac.kr

✉ Tae-Joon Jeon
tjjeon@inha.ac.kr

1 Department of Biological Sciences and Bioengineering, Inha University, Incheon 22212, South Korea

2 Biohybrid Systems Research Center (BSRC), Inha University, Incheon 22212, South Korea

3 Department of Chemical Engineering, Dankook University, Yongin 16890, South Korea

4 Department of Biological Engineering, Inha University, Incheon 22212, South Korea

5 Department of Mechanical Engineering, Inha University, Incheon 22212, South Korea

fluid by 11 s [14]. In other studies, He et al. reported dissoluble saline barriers for controlling the fluid flow [15], and Lutz et al. showed that the addition of sucrose delayed the flow of fluid [16]. Through these various studies, chemical and physical control of viscosity is one way to effectively increase the signal readout.

In this study, to further increase the signal readout, we devised an LFA assay with a superabsorbent polymer (SAP)-coated membrane by increasing the viscosity of the fluid. SAP, used in various fields (hygienic, agriculture, food packaging, etc.) [17], is a hydrophilic polymer that can absorb and hold a large amount of liquid relative to its own mass through hydrogen bonding with water molecules [18, 19]. Oyama et al. proposed that the absorption capacity of SAP can control the flow of fluid for acrylic POCT devices [20]. Biswas et al. described a micropump using a freeze-dried disc of SAP. This SAP disc pump could facilitate automatic processing for bioassays and is used for controlling absorption [19].

In contrast to the previously proposed SAP-modified papers, we devised a method to increase the sensitivity by increasing the viscosity of the transporter by using SAP in the process of analyte migration. This technique intentionally reduces the fluid flow of the sample. When precoated SAP is mixed with the migrating analytes, the viscosity changes, and the flow rate is controlled to further extend the reaction time. SAP is simply spread on the porous membrane rather than applied as a pretreatment by mixing the samples with SAP, making it more suitable for POCT. Through this method, the sensitivity and signal readout improved more than three times compared to basic LFAs because of the effective delay of the coupling reaction time in both the test line and control line. As a result, our work shows a more sensitive LFA platform, where the flow of fluid is effectively delayed by a simple coating of SAP. To maximize signal enhancement, the concentration of SAP solution was optimized mathematically (fluid saturation and molecular dynamic simulations) and experimentally. As a result, our device provides an easily fabricable LFA platform with enhanced signal readouts; thus, test results can be seen simply with the naked eye.

Experimental

Materials and reagents

Chloroauric acid ($HAuCl_4$), goat anti-human IgG (whole molecule), goat anti-human IgG (γ-chain specific)-biotin, human IgG from human serum, citric acid trisodium salt dihydrate, monopotassium phosphate, Tween 20, and bovine serum albumin (BSA) were purchased from Sigma-Aldrich (Korea). Chicken anti-goat IgG was purchased from Abcam (UK). Human immunoglobulin (IgG, IgA, IgM and IgE)-depleted serum was purchased from Celprogen (Torrance, CA, USA). Sodium polyacrylate (polymerization degree 22,000–70,000) was purchased from Fujifilm Wako Pure Chemical Corp. Polyvinyl alcohol (PVA) 500, sucrose, and potassium carbonate were purchased from Junsei Chemical Co., Ltd. (Tokyo, Japan). All materials for LFA chip manufacturing were purchased from Bore Da Biotech Co., Ltd. (Seongnam, Korea): the absorbent pad, nitrocellulose (NC) membrane, sample pad, conjugate pad, and backing card. COMSOL 5.5 software based on multiphase flow at the porous media interface was used for mathematical simulations.

AuNP conjugation with antibodies

AuNPs were conjugated to antibodies with a slight modification of the previously reported method [21]. First, the AuNP suspension in 0.1 M borate buffer was adjusted to pH 7 using 0.25 M K_2CO_3 solution. Twenty microliters of goat anti-human IgG (γ-chain specific)-biotin aqueous solution was added to 1 mL of AuNP suspension. Then, 100 µL of BSA aqueous solution (1% w/v) was added and incubated at 650 rpm for an additional 20 min. Finally, the solution was centrifuged at 10,000 rpm and 4 °C for 20 min. The supernatant was removed, and the AuNP/anti-human IgG pellet was resuspended in 500 µL of borate buffer (2 mM, pH 7.4, 5% w/v sucrose). To determine the minimum antibody concentration, the conjugated AuNPs were then characterized with a gold aggregation test (Figure S2).

Fabrication of lateral flow test strips

Prior to assembling the components of the test strip, we prepared the sample pad by immersing in 10 mM PBS, 5% BSA and 0.05% Tween 20 and drying it at 60 °C for 2 h. The conjugate pad was submerged in 0.05% PVA and 0.05% Tween 20 for 24 h and then completely dried in place. Next, the conjugate pad was functionalized with AuNP/anti-human IgG dispersion and desiccated overnight. Then, 1 mg mL^{-1} goat anti-human IgG (whole molecule) and chicken anti-goat IgG solutions were fixed on the test lines and control lines, respectively. The NC membrane was modified by adding various volumes and concentrations of SAP to the empty area near the conjugate pad and then dried at 37 °C for 1 h. The prepared sample pad, conjugate pad, NC membrane, and absorbent pad were assembled on the backing card. Then, the assembled card was cut into 4-mm strips using a guillotine paper cutter.

Assay procedure

To investigate the effect of SAP on detection sensitivity and retention time, test strips were modified with different SAP concentrations (0.05%, 0.1%, 0.25%, 0.5%, 1% w/v). The sample pad was immersed in 100 µL of diluted human IgG in PBS (10 mM, pH 7.4) ranging from 10 to 500 ng mL-1 for 20 min. During the experiment, images were taken with an iPhone 8 (Apple Inc., CA, USA), and the optical signal was obtained from the captured images. The obtained signals were further converted to grayscale for quantitative analysis using ImageJ software. All tests were repeated three times to verify the reliability of our experiments. In addition, spiked samples using human immunoglobulin-depleted serum were tested in the same way.

Mathematical simulations

The flow can be studied using the extended Darcy's law, which describes the effects of fluid dynamic viscosity and pressure [22–24]. Inspired by previous works, the mathematical model was simplified to include only the NC membrane, atmospheric saturation, and water pressure [22]. We assumed that SAP had no effect on the porous structure and pore size and considered only the fluid dynamic viscosity and capillary action affected by SAP. The paper strip was initially filled with 0.99 air. In the case of phase transport, no flux was assumed for the air phase at the bottom boundary, and the mass flow velocity in the air due to the pressure gradient given in the Darcy model at the upper boundary was defined. We used this assumption and the well-known Darcy's law to obtain the following equation:

$$Q = \frac{kA}{\mu}\Delta P \tag{1}$$

where Q is the volume flow rate, µ is the viscosity of the fluid, κ is the permeability of the porous medium to the fluid, A is the cross-sectional area of the flow, and ΔP is the pressure drop per unit length of the porous medium. According to Darcy's law, the volumetric flow rate is inversely proportional to the viscosity. Consequently, the dynamic viscosity of different pads and fluid saturation over time can be estimated.

Molecular dynamics simulations

All simulations and analyses were performed using the GROMACS-2018 simulation package [25–27] with the CHARMM force field [28, 29]. The coordinates and potential parameters of SAP, which consists of 30 acrylic acids per chain, were generated from CHARMM-GUI [30]. Five SAP molecules were randomly positioned and solvated with ~ 3440 TIP3P waters [31] in a periodic box of size 4.8 nm/side. Since each SAP has a net charge of -30, 150 counterions (Na +) were added to neutralize the system. For comparison, pure water molecules without SAP were also simulated. A temperature of 298 K and a pressure of 1 bar were maintained by applying a velocity-rescale thermostat [32] and Parrinello-Rahman barostat [33] in an NPT ensemble. The Lennard–Jones potential was smoothly shifted to zero between 1.0 and 1.2 nm, while the short-range electrostatic cutoff of 1.2 nm was supplemented by a particle mesh Ewald summation for long-range electrostatics [34]. The LINCS algorithm was used to constrain the bond lengths [35, 36]. Simulations were performed for 30 ns with a time step of 2 fs on computational facilities supported by the National Institute of Supercomputing and Networking/Korea Institute of Science and Technology Information with supercomputing resources including technical support (KSC-2020-CRE-0095). The last 20 ns trajectories were used to calculate solvent diffusivities.

Results and discussion

Controlling fluid on the SAP-coated membrane

In this study, we developed a simple strategy that is applicable to general LFA tests with improved sensitivity by combining SAP with a typical LFA strip. A sandwich ELISA (enzyme-linked immunosorbent assay) is used for the technique in LFA strips and gold nanoparticles (AuNPs) are used as its recognition agent (Figure S1). This technique uses two antibodies, namely, detection and capture antibodies, targeting different epitopes of the same antigen. The antigen and capturing antibodies were conjugated, and then the conjugates were combined with the detection antibody. In this study, the strip had four stages with different pads. First, the sample was dropped onto the end of the strip with the sample pad. PBS, BSA, and Tween-20 in the sample pad made the sample suitable for the LFA strip (Fig. 1A). Then, the applied sample migrated to the conjugate pad by capillary force. As the sample arrived at the conjugate pad, the sample was specifically bound to the anti-human IgG tagged with AuNPs (Fig. 1B). Once it arrived at the NC membrane, the solution started to flow slowly due to the membrane pretreated with SAP (Fig. 1C). The low-density cross-linked SAP absorbed in the LFA between the conjugate pad and the test line decreased the flow rate while increasing the reaction time of biomolecules and the color intensity of the test line (Fig. 1D).

When dry SAP is immersed in water, it expands 2 to 3 times, and its ability to swell is crucial in practical applications, including agricultural and hygienic uses. In addition, SAP has high water absorption capacity and water

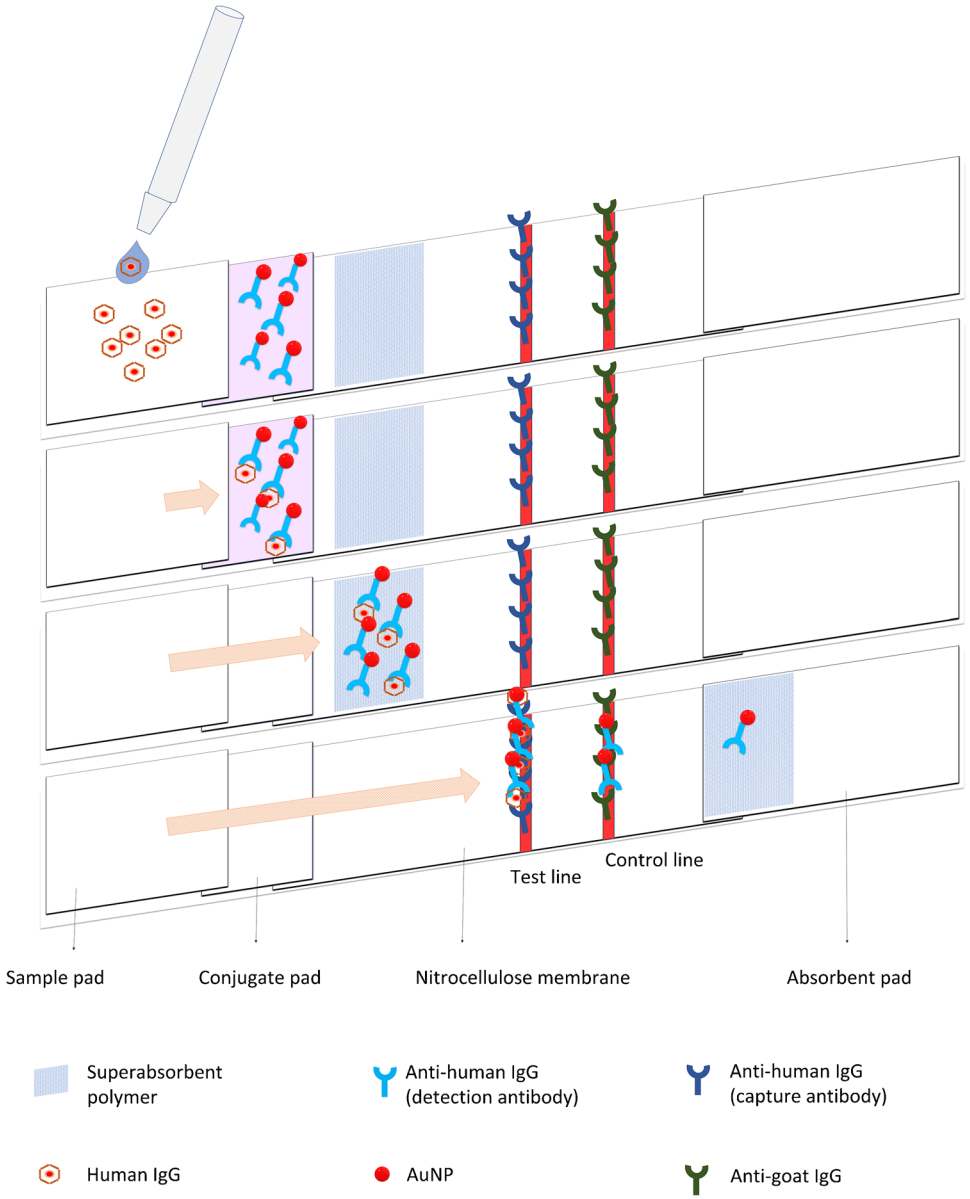

Fig. 1 Schematic illustration of the strategy of sensitivity enhancement by SAP based on LFA. (**a**) Dropping of the sample onto the end of the strip with the sample pad. (**b**) Migration of the applied sample bound to the anti-human IgG tagged with AuNPs in the conjugate pad. (**c**) NC membrane pretreated with SAP. (**d**) Binding of the analytes to the test line and control line

uptake is as much as 1000 times of its own weight [17]. High-density cross-linked SAPs are more commonly used because they have stronger gel strength and can maintain the shape of gel even under pressure, but low-density cross-linked SAPs have gel-forming characteristics with a fast absorption time and high viscosity [37, 38]. Considering the characteristics of LFAs, which enable the rapid detection of target molecules with excellent sensitivity, we first selected sodium polyacrylate, a low-density crosslinked SAP. For rapid and desirable fluid control, a volume of SAP (3 µL) suitable to completely cover one line of the NC membrane was used. Then, we tried to find the optimum concentration after evaluating the effect of SAP on LFA. Five different concentrations of SAP (0.05%, 0.1%, 0.25%, 0.5%, and 1% w/v) were added to the NC membrane (Fig. 2). After SAP immobilization, an increase in color intensity was observed in the test line due to controlled fluid flow. As the added SAP ratio increased, the color intensity of the test line tended to increase and become more concentrated.

Optimization of SAP concentration

After each modification process, we characterized the morphological structure of the membrane by SEM to confirm the interaction between SAP and the NC membrane. The strip was freeze-dried from the reaction until the SEM image was taken. In the NC membranes, regardless of whether they were unmodified or modified with 0.5% SAP or less, the average pore diameter was homogeneous at

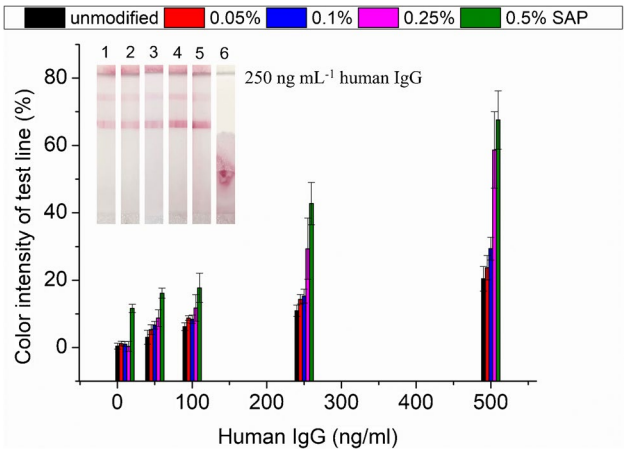

Fig. 2 Effect of SAP on test strips. Quantitative analysis for the detection of human IgG performed with the different human IgG concentrations on test strips in various SAP concentrations (unmodified, 0.05%, 0.1%, 0.25%, and 0.5% SAP, respectively). Inset: photographs of LFA strips used to detect 250 ng mL-1 human IgG (1–6: unmodified, 0.05%, 0.1%, 0.15%, 0.5% and additional 1% SAP, respectively)

17.18 ± 4.27 nm, and no morphological change or damage to the membrane was observed (Figure S3). That is, the pore size did not change with respect to SAP concentrations, showing that SAP did not affect the porous structure of the membrane other than the viscosity of the fluid. However, as shown in Fig. 2, background noise was observed in the NC membrane treated with SAP at a high concentration over 1%, suggesting that the movement of molecules was hindered as the dynamic viscosity of the fluid increased, while the reaction time further increased due to the relatively high dynamic viscosity of the fluid and the flow delay (inset in Fig. 2). As a result, analytes and AuNP/antibody conjugates in the loading sample did not completely travel through the NC membrane, which was not suitable for LFA. Figure 2 shows that the normalized intensity of color signals increased as the concentrations of human IgG increased. Response histograms and saturation channels from 10 to 500 ng mL-1 (due to the Hook effect, no concentration increases over 500 ng mL-1) were performed to investigate the improvement in sensitivity obtained under each condition. We calibrated the color intensity measurement by subtracting the average brightness of the background noise from the signal intensity. Moreover, strips treated with high concentrations of SAP (more than 1% SAP), where little fluid flowed, were excluded. In summary, higher sensitivity was achieved when using higher SAP concentrations over the entire range of human IgG concentrations tested. The highest sensitivity while maintaining fluid flow to the control line was obtained for 0.5% SAP-modified LFA, which increased signals up to 10 times compared to those obtained in the unmodified LFA.

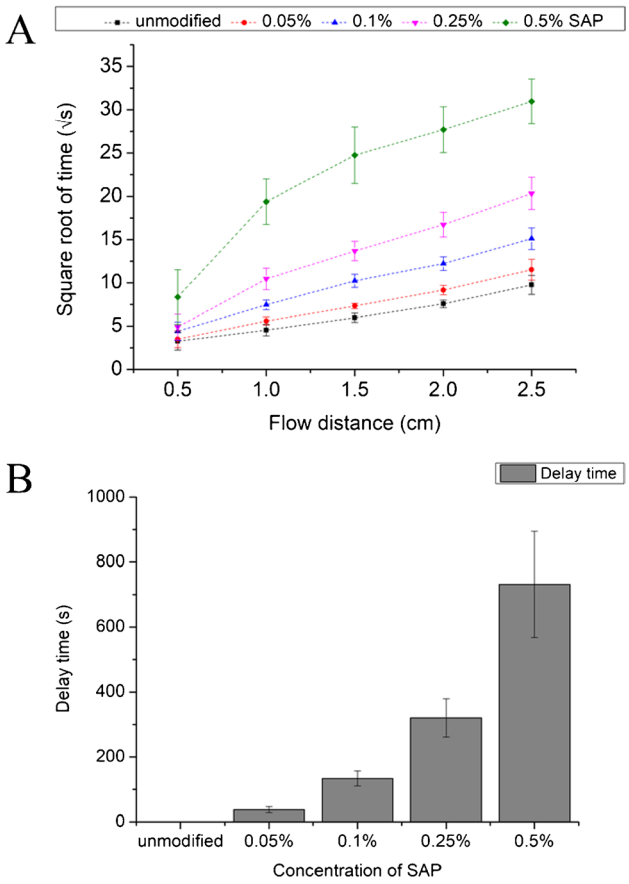

Fig. 3 Effect of SAP concentration on fluid flow. (**a**) Relationship between flow distance with different SAP concentrations and the square root of time. (**b**) Bar graph for quantitative delay time with different concentrations of SAP

Optimization of the assay time

When developing a rapid test kit, the time required for testing is one of the most important parameters to be optimized. According to the initial conditions optimized above, we further investigated flow control with various concentrations of SAP. The total assay time was measured from the moment the sample was loaded on the nitrocellulose membrane until it passed through the absorbent pad. We calculated the delay time by measuring the wicking distance of AuNPs through the nitrocellulose membrane at 0.5-cm intervals. As shown in Fig. 3A, the flow rate decreased immediately at the 0.5–1.0 cm flow distance where SAP was treated, and the flow rate was continuously affected even after the sample flowed past the SAP region. The optimal flow time delay was obtained when using 0.5% SAP, which resulted in a flow time of 731 s (Fig. 3B) without halting the fluid flow before it reached the absorbent pad. As expected, the LFA wicking distance results indicated that the flow rate gradually decreased with increasing SAP concentration. To better

understand the mechanism of fluid flow in the paper strip, we built a mathematical model to simulate fluid saturation and delay time through the nitrocellulose membrane of LFA (Figure S4). We found that the SAP-modified LFA delayed fluid saturation over time (10, 50, 100, 200, 300, 600 s) compared to the unmodified LFA. The reaction time was delayed up to 5 min due to the slowed fluid flow. This result showed a similar tendency to the experimental results and proved that increasing the dynamic viscosity of the fluid can slow the flow rate in LFA.

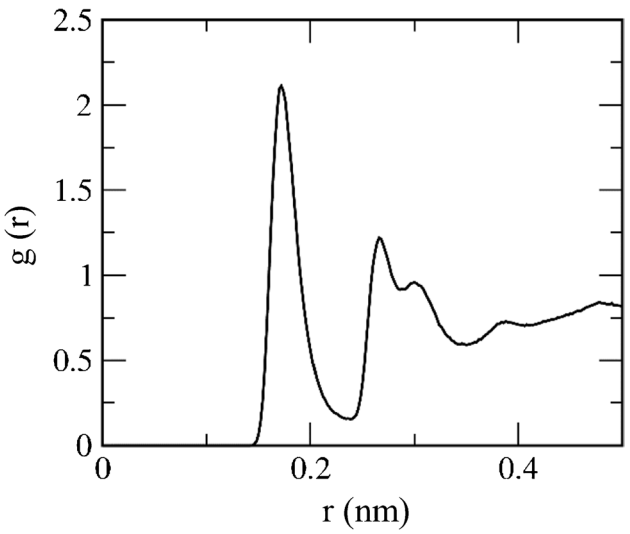

Fig. 4 RDF between water and the hydroxyl group of SAP

Molecular dynamics simulations: the effect of SAP on solvent viscosity

To understand the effect of SAP on the solvent viscosity, we performed molecular dynamics simulations and compared the diffusivities of water with and without SAP. To obtain diffusion coefficients, the slope of the mean-square displacement of water was calculated, showing that the diffusivities of water with and without SAP were 3.05 ± 0.01 and 5.60 ± 0.01 ($\times 10^{-5}$) $cm^2\ s^{-1}$, respectively. This, combined with the Stokes–Einstein relationship [39], indicated that the presence of SAP significantly increased the solvent viscosity, in agreement with experiments. To understand the effect of the SAP-water interaction, the radial distribution function (RDF) between water and the hydroxyl group of SAP was calculated, showing a sharp peak at approximately 0.17 nm (Fig. 4). These findings indicated that the hydroxyl groups of SAP strongly interact with water molecules and thus reduce the water diffusivity, which helps explain the experimental observation of increased water viscosity in the presence of SAP.

Detection of human IgG from spiked samples

To investigate compatibility with real samples, we performed a validation test using human immunoglobulin-depleted serum (Fig. 5). In previously reported studies, human serum samples are commonly used in validation assays to establish reliability [13, 40]. The spiking recoveries of human IgG in the samples ranged from 86.79 to 122.43% at three concentrations of 100, 300, and 1000 ng mL^{-1} [13]. We compared unmodified LFAs with 0.5% SAP-modified LFAs, which provided the highest sensitivity, based on IgG-spiked human serum at varying

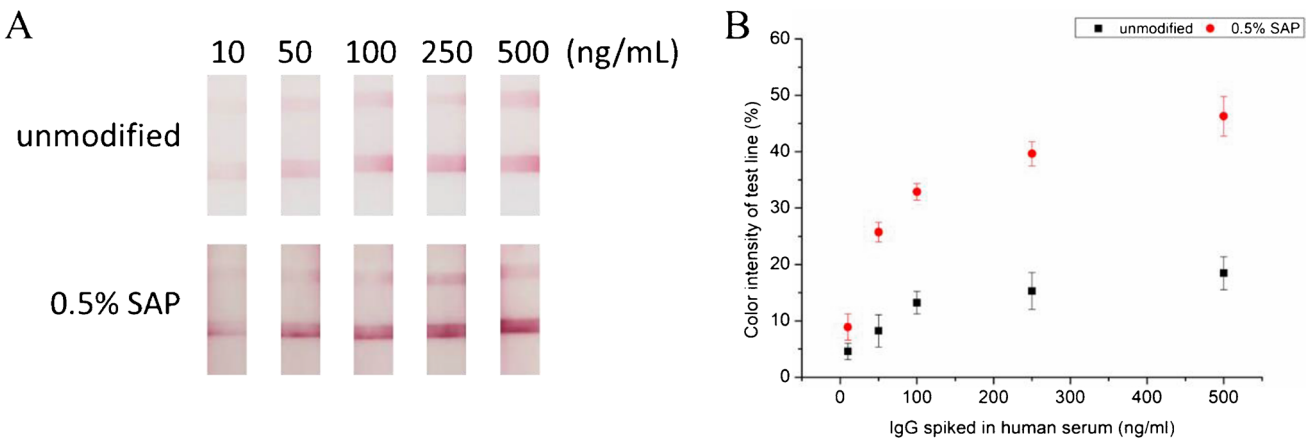

Fig. 5 Detection results of the test strips with spiked human serum. (**a**) Photographic images of the validation of different concentrations of spiked human serum of the control and test lines. (**b**) A quantitative graph of the color intensity of the test line with spiked human serum

concentrations of 10–500 ng mL^{-1}. Similar saturated channels of the two samples were formed as the analyte concentration increased because of the hook effect that often occurs in sandwich assays [41]. Overall, the binding signal tended to be high in LFAs treated with 0.5% SAP in all ranges tested, and no readout errors or nonspecific binding were observed. This indicates that the complex nature of human serum did not affect the SAP-treated LFA results.

Conclusion

We proposed a simple strategy to improve the sensitivity of an LFA-based biosensor using SAP. Using 0.5% SAP, it is possible to obtain the optimum dynamic viscosity generated by the interaction of SAP and the loading sample and to provide a reaction time for the optimal interaction of biomolecules. The time for reaction was delayed up to 5 min, which may be a minor limitation, but is still suitable for general POCT use. Moreover, these experimental results were confirmed through mathematical modeling and molecular dynamics simulations. This approach significantly improved the degree of reaction between human IgG and AuNP/antibody conjugates, as the optical signal was amplified up to 10 times compared to that in conventional LFA. The device modified with low-density crosslinked SAP shares the same usage and manufacturing format as existing LFAs, thereby achieving timely delivery of secondary reagents with a simple method. To the best of our knowledge, our approach to enhance the sensitivity by applying SAP to LFAs is reported first; thus we believe that this approach can be applied to point-of-care biosensors because it does not require the use of additional reagents or complex equipment for signal amplification. In addition, given the high sensitivity, our ongoing research includes the application of our sensing platform to virus detection where more enhanced sensitivity is required.

Supplementary Information The online version contains supplementary material available at https://doi.org/10.1007/s00604-021-05026-2.

Acknowledgements This work was carried out with the support of the ''Cooperative Research Program for Agriculture Science and Technology Development (Project No. PJ014238042021)" Rural Development Administration, Republic of Korea, as well as the Inha University Research Grant.

Declarations

Conflict of interest The authors declare no competing interests.

References

1. Jung W, Han J, Choi JW, Ahn CH (2015) Point-of-care testing (POCT) diagnostic systems using microfluidic lab-on-a-chip technologies. Microelectron Eng 132:46–57. https://doi.org/10.1016/j.mee.2014.09.024
2. Gong MM, Sinton D (2017) Turning the page: advancing paper-based microfluidics for broad diagnostic application. Chem Rev 117:8447–8480. https://doi.org/10.1021/acs.chemrev.7b00024
3. Wu G, Zaman MH (2012) Low-cost tools for diagnosing and monitoring HIV infection in low-resource settings. Bull World Health Organ 90:914–920. https://doi.org/10.2471/BLT.12.102780
4. Li F, You M, Li S et al (2019) Paper-based point-of-care immunoassays: Recent advances and emerging trends. Biotechnol Adv. https://doi.org/10.1016/j.biotechadv.2019.107442
5. Xiong X, Zhang J, Wang Z et al (2020) Simultaneous multiplexed detection of protein and metal ions by a colorimetric microfluidic paper-based analytical device. Biochip J 14:429–437. https://doi.org/10.1007/s13206-020-4407-9
6. Hyung S, Karima G, Shin K et al (2021) A simple paper-based α-amylase separating system for potential application in biological sciences. Biochip J. https://doi.org/10.1007/s13206-021-00022-3
7. Hidayat MA, Maharani DA, Purwanto DA et al (2020) Simple and sensitive paper-based colorimetric biosensor for determining total polyphenol content of the green tea beverages. Biotechnol Bioprocess Eng 25:255–263. https://doi.org/10.1007/s12257-019-0299-8
8. Lim SH, Ryu YC, Hwang BH (2021) Aptamer-immobilized gold nanoparticles enable facile and on-site detection of staphylococcus aureus. Biotechnol Bioprocess Eng 26:107–113. https://doi.org/10.1007/s12257-020-0161-z
9. Koczula KM, Gallotta A (2016) Lateral flow assays. Essays Biochem 60:111–120. https://doi.org/10.1042/EBC20150012
10. Quesada-González D, Merkoçi A (2015) Nanoparticle-based lateral flow biosensors. Biosens Bioelectron 73:47–63. https://doi.org/10.1016/j.bios.2015.05.050
11. Carrilho E, Martinez AW, Whitesides GM (2009) Understanding wax printing: A simple micropatterning process for paper-based microfluidics. Anal Chem 81:7091–7095. https://doi.org/10.1021/ac901071p
12. Renault C, Koehne J, Ricco AJ, Crooks RM (2014) Three-dimensional wax patterning of paper fluidic devices. Langmuir 30:7030–7036. https://doi.org/10.1021/la501212b
13. Sena-Torralba A, Ngo DB, Parolo C et al (2020) Lateral flow assay modified with time-delay wax barriers as a sensitivity and signal enhancement strategy. Biosens Bioelectron 168:112559. https://doi.org/10.1016/j.bios.2020.112559
14. Preechakasedkit P, Siangproh W, Khongchareonporn N et al (2018) Development of an automated wax-printed paper-based lateral flow device for alpha-fetoprotein enzyme-linked immunosorbent assay. Biosens Bioelectron 102:27–32. https://doi.org/10.1016/j.bios.2017.10.051
15. He X, Liu Z, Yang Y et al (2019) Sensitivity enhancement of nucleic acid lateral flow assays through a physical-chemical coupling method: dissoluble saline barriers. ACS Sensors 4:1691–1700. https://doi.org/10.1021/acssensors.9b00594
16. Lutz B, Liang T, Fu E et al (2013) Dissolvable fluidic time delays for programming multi-step assays in instrument-free paper diagnostics. Lab Chip 13:2840–2847. https://doi.org/10.1039/c3lc50178g

17. Zohuriaan-Mehr MJ, Kabiri K (2008) Superabsorbent polymer materials: A review. Iran Polym J English Ed 17:451–477
18. Zohuriaan-Mehr MJ, Omidian H, Doroudiani S, Kabiri K (2010) Advances in non-hygienic applications of superabsorbent hydrogel materials. J Mater Sci 45:5711–5735. https://doi.org/10.1007/s10853-010-4780-1
19. Biswas GC, Rana MM, Kazuhiro T, Suzuki H (2019) A simple micropump based on a freeze-dried superabsorbent polymer for multiplex solution processing in disposable devices. R Soc Open Sci 6(3):182213. https://doi.org/10.1098/rsos.182213
20. Oyama Y, Osaki T, Kamiya K et al (2017) A sensitive point-of-care testing chip utilizing superabsorbent polymer for the early diagnosis of infectious disease. Sensors Actuators, B Chem 240:881–886. https://doi.org/10.1016/j.snb.2016.09.046
21. Ambrosi A, Castañeda MT, Killard AJ et al (2007) Double-codified gold nanolabels for enhanced immunoanalysis. Anal Chem 79:5232–5240. https://doi.org/10.1021/ac070357m
22. Masoodi R, Pillai KM (2010) Darcy's law-based model for wicking in paper-like swelling porous media. AIChE J 59:NA-NA. https://doi.org/10.1002/aic.12163
23. Parolo C, Medina-Sánchez M, de la Escosura-Muñiz A, Merkoçi A (2013) Simple paper architecture modifications lead to enhanced sensitivity in nanoparticle based lateral flow immunoassays. Lab Chip 13:386–390. https://doi.org/10.1039/C2LC41144J
24. Liu M, Suo S, Wu J et al (2019) Tailoring porous media for controllable capillary flow. J Colloid Interface Sci 539:379–387. https://doi.org/10.1016/j.jcis.2018.12.068
25. Hess B, Kutzner C, Van Der Spoel D, Lindahl E (2008) GRGMACS 4: Algorithms for highly efficient, load-balanced, and scalable molecular simulation. J Chem Theory Comput 4:435–447. https://doi.org/10.1021/ct700301q
26. Lindahl E, Hess B, van der Spoel D (2001) GROMACS 3.0: A package for molecular simulation and trajectory analysis. J Mol Model 7:306–317. https://doi.org/10.1007/S008940100045
27. Van Der Spoel D, Lindahl E, Hess B et al (2005) GROMACS: Fast, flexible, and free. J Comput Chem 26:1701–1718. https://doi.org/10.1002/jcc.20291
28. Brooks BR, Brooks CL, Mackerell AD et al (2009) CHARMM: The biomolecular simulation program. J Comput Chem 30:1545–1614. https://doi.org/10.1002/jcc.21287
29. Brooks BR, Bruccoleri RE, Olafson BD, States DJ, Swaminathan S, Karplus M (1983) Charmm - a program for macromolecular energy, minimization, and dynamics calculations. J Comput Chem 4:187–217
30 Sunhwan JO, Taehoon KIM, Vidyashankara G, Iyer WI (2008) CHARMM-GUI: A Web-Based Graphical User Interface for CHARMM. J Comput Chem 29:1859–1865. https://doi.org/10.1002/jcc
31. Jorgensen WL, Chandrasekhar J, Madura JD et al (1983) Comparison of simple potential functions for simulating liquid water. J Chem Phys 79:926–935. https://doi.org/10.1063/1.445869
32. Bussi G, Donadio D, Parrinello M (2007) Canonical sampling through velocity rescaling. J Chem Phys 126(1):014101. https://doi.org/10.1063/1.2408420
33. Parrinello M, Rahman A (1981) Polymorphic transitions in single crystals: A new molecular dynamics method. J Appl Phys 52:7182–7190
34. Essmann U, Perera L, Berkowitz ML et al (1995) A smooth particle mesh Ewald method. J Chem Phys 103:8577–8593. https://doi.org/10.1063/1.470117
35. Hess B (2008) P-LINCS: A parallel linear constraint solver for molecular simulation. J Chem Theory Comput 4:116–122. https://doi.org/10.1021/ct700200b
36. Hess B, Bekker H, Berendsen HJC, Fraaije JGEM (1997) LINCS: A Linear Constraint Solver for molecular simulations. J Comput Chem 18:1463–1472. https://doi.org/10.1002/(SICI)1096-987X(199709)18:12%3c1463::AID-JCC4%3e3.0.CO;2-H
37. Omidian H, Hashemi SA, Sammes PG, Meldrum I (1999) Modified acrylic-based superabsorbent polymers (dependence on particle size and salinity). Polymer (Guildf) 40:1753–1761. https://doi.org/10.1016/S0032-3861(98)00394-2
38. Sawut A, Yimit M, Sun W, Nurulla I (2014) Photopolymerisation and characterization of maleylatedcellulose-g- poly(acrylic acid) superabsorbent polymer. Carbohydr Polym 101:231–239. https://doi.org/10.1016/j.carbpol.2013.09.054
39. Fredrickson GH (1996) The theory of polymer dynamics. Curr Opin Solid State Mater Sci 1:812–816. https://doi.org/10.1016/S1359-0286(96)80106-9
40. Cheeveewattanagul N, Morales-Narváez E, Hassan ARHA et al (2017) Straightforward immunosensing platform based on graphene oxide-decorated nanopaper: a highly sensitive and fast biosensing approach. Adv Funct Mater 27:1–8. https://doi.org/10.1002/adfm.201702741
41. Gao Y, Zhu Z, Xi X et al (2019) An aptamer-based hook-effect-recognizable three-line lateral flow biosensor for rapid detection of thrombin. Biosens Bioelectron 133:177–182. https://doi.org/10.1016/j.bios.2019.03.036